Processing and Application of Ceramics 12 [1] (2018) 78–85
https://doi.org/10.2298/PAC1801078A

Comparative structural and optical spectroscopic studies of Nd^{3+} ion doped LaF_3 and their core/shell nanoparticles

Anees A. Ansari[1,*], Joselito P. Labis[1], Mohamed Aslam Manthrammel[2]

[1]*King Abdullah Institute for Nanotechnology, King Saud University, Riyadh-11451, Saudi Arabia*
[2]*Department of Physics, College of Sciences, King Saud University, Riyadh-11451, Saudi Arabia*

Received 30 November 2017; Received in revised form 25 February 2018; Accepted 14 March 2018

Abstract

LaF_3:Nd^{3+} (core), LaF_3:Nd^{3+}@LaF_3 (core/shell) and LaF_3:Nd^{3+}@LaF_3@SiO_2 (core/shell/SiO_2) nanoparticles (NPs) were designed and synthesized at low temperature. The structure and morphology of the as-prepared nanoproducts were characterized by X-ray diffraction and transmission electron microscopy (TEM) techniques. Thermal analysis and FTIR spectral studies were conducted to examine the surface properties of the nanomaterials. The as-prepared LaF_3:Nd^{3+} NPs exhibited hexagonal structure and were composed of monodispersed irregularly and spherically shaped NPs with average grain size of 21 nm. TEM image showed the successful silica surface coating, which was verified by FTIR spectral analysis. The emission spectra of LaF_3:Nd^{3+} NPs was obtained by monitoring the emission of Nd^{3+} at 325 nm (Cd laser) where it exhibited the characteristic $4f \rightarrow 4f$ transitions lines originating from the Nd $4f^3$ configuration. Under UV light irradiation, the emission spectra revealed various strong emission transitions which were greatly affected by the surrounding silica surface coating. These observed results suggested future applications in biolabeling and light-emitting diode.

Keywords: *neodymium, lanthanum fluoride, thermal analysis, optical energy band gap, photoluminescence*

I. Introduction

Neodymium ion-doped nanomaterials have attracted reviving research interest due to their near-infrared (NIR) emission characteristics [1–10]. Furthermore, these Nd ion-doped nanomaterials have come to the forefront in nanophotonics owing to their distinct electrical, optical and magnetic properties and found potential applications in diversed fields such as in light emitting diode, lasers, luminescent bio-labeling/optical bio-probes and bio-imaging [1,2,4,8]. Nd^{3+} ions have been extensively used in the laser crystals since it has abundant pumping levels, a 4-level scheme having both relatively high absorption and emission cross sections. These exceptional properties of Nd^{3+} ion-doped nanomaterials arise from the fact that their optical transitions take place among internal $4f$-orbitals which are shielded from the environment by the $5d$-orbital electrons [11–13]. It results in a narrow emission band with extremely stable wavelength regardless to certain extent of the external conditions in the matrix and transparent in the wide spectral range. Nd^{3+} ions possess $4f^25d \rightarrow 4f^3$ spin-allowed transitions with fast response covering the spectral range 400–2000 nm wavelengths [2,7,10]. Additionally, multiple $4f^3 \rightarrow 4f^3$ spin forbidden transitions with slow decay in the range from 400 to 900 nm were also reported [2,10.14]. In most cases, optical bio-detection/bio-probe required fast response. Therefore, Nd^{3+} ion-doped nanomaterials that have wider transparency region are expected to be a fast-response luminescent bio-detector, which is attributed to $4f^25d \rightarrow 4f^3$ spin allowed transition [2,7,10]. By contrast, researches regarding slow response emission that originates from $4f^3 \rightarrow 4f^3$ spin forbidden transitions have not been carried out sufficiently and that motivated us to examine the luminescence properties following from the $4f^3 \rightarrow 4f^3$ spin forbidden transition in Nd^{3+} doped nanomaterials.

On the other hand, LaF_3 was used as a host matrix of Nd^{3+} ions [6,8,9,15]. This material is a well-known host material for various phosphors because it has very low phonon energy and, thus, the quenching of the excited state of the lanthanide ions is minimal [9]. Therefore, this material is a promising nano

*Corresponding author: tel: +966 1 4676838,
fax: +966 1 4670662, e-mail: *aneesaansari@gmail.com*

phosphor matrix for next generation optoelectronic devices working in longer wavelengths. Due to its low phonon energy and high refractive index, it is expected to provide significantly high-radiative decay rates and low non-radiative relaxation rates of lanthanide excited state levels. The preparation and optical properties of Nd^{3+}-ion doped LaF_3 nanomaterials have been investigated extensively [9,16]. Sivakumar *et al.* prepared various mono-dispersed lanthanide (Ln = Nd, Eu, Tb and Er) ion-doped LaF_3 nanocrystals [9]. In another report, the solvothermal route was utilized for Nd ion doping into the LaF_3 crystal lattice [17]. Cui *et al.* [15] introduced Nd ions into the LaF_3 crystal lattice through co-precipitation method to investigate their luminescent character. Luo *et al.* [18] synthesized $LaF_3:Nd^{3+}$ NPs (NPs) via the hydrothermal method and investigated the effect of different ligands on luminescent properties of the as-prepared NPs. Previous reports also indicate that processable nanostructures doped with infrared-emitting lanthanides are of particular interest as active materials in biomedical sciences, lasers and light emitting diodes [7,9,10,16]. To the best of our knowledge, this is first report that investigates the down-conversion luminescent properties of Nd^{3+}-ion doped LaF_3 NPs on excitation from low wavelength to get emissions in the visible region. As part of an ongoing investigation into the down-conversion luminescence of Nd^{3+} ion-doped LaF_3 NPs, well-aqueous dispersible, irregular and spherical shaped nanostructures were prepared by a simple one-pot co-precipitation process in the presence of ethylene glycol as a chelating agent. However, it has been reported that the luminescent efficiency of lanthanide ions were quenched dramatically when incorporated into NPs, which could be due to the large surface-to-volume ratio of NPs causing a number of dopant luminescent ions to reside on the NPs surface, which then forms surface defects and thus hampers optical efficiency [19,20]. These surface ions would absorb some groups, such as −OH, −NH and −CH, which also noticeably quench the emissions of luminescent ions. In order to reduce these surface defects, similar insulating crystalline inorganic shells have been introduced to shield the lanthanide ions and therefore created the so-called core/shell nanostructure. However, weak solubility in an aqueous environment has become the main drawback of these core/shell structured nanomaterials and the silica surface coating over these luminescent core/shell NPs has found as an attractive alternate to overcome this drawback and improve solubility and colloidal stability in an aqueous solvent for applications in biomedical sciences [9,21,22]. These core, core/shell and core/shell/SiO_2 NPs display several non-overlapping emission lines that cover the visible-to-near infrared region (400–800 nm) through down-conversion process.

In this study, comparative structural, thermal, optical band gap and photoluminescence properties are demonstrated and the effects of surface coating on crystallinity, energy band gap and emission properties are further investigated.

II. Experimental

2.1. Materials

La_2O_3 (99%, BDH, UK), Nd_2O_3 (99.99%, Alfa Aesar, Germany), ethanol (E-Merck, Germany), tetraethylorthosilicate (TEOS, 99 wt.% analytical reagent A.R.), ethylene glycol (EG), HNO_3 and NH_4OH were used as the starting materials without any further purification. $La(NO_3)_3{\times}6\,H_2O$ and $Nd(NO_3)_3{\times}6\,H_2O$ were prepared by dissolving the corresponding oxides in diluted nitric acid. The double distilled H_2O was prepared using a Milli-Q system (Millipore, Bedford, MA, USA).

2.2. Preparation of $LaF_3:Nd^{3+}$ NPs

For the preparation of Nd^{3+}-doped LaF_3 NPs ($La_{0.99}Nd_{0.01}F_3$), 0.2 M stock solutions of $La(NO_3)_3{\times}6\,H_2O$ and $Nd(NO_3)_3{\times}6\,H_2O$ in de-ionized water were prepared. Briefly, 9.9 ml of $La(NO_3)_3{\times}6\,H_2O$ and 0.1 ml of $Nd(NO_3)_3{\times}6\,H_2O$ were dissolved in 50 ml of EG. An equal molar aqueous solution of NH_4F was then added drop-wise under magnetic stirring. The whole solution was kept on a hotplate at 80 °C under magnetic stirring to obtain a homogenous mixture. This homogeneously mixed solution was transferred to a 250-ml round bottle flask fitted with a reflux condenser for 4 h until complete precipitation. After cooling to room temperature, the white precipitate was segregated to the bottom. The product was collected by centrifugation, washed with distilled water and C_2H_5OH several times, and dried in an oven at 60 °C for 6 h.

2.3. Preparation of $LaF_3:Nd^{3+}@LaF_3$ NPs

For the preparation of $LaF_3:Nd^{3+}@LaF_3$ core/shell NPs, similar polyol process was used as discussed above. The as-prepared 0.500 g LaF_3:Nd was dispersed with the help of ultra-sonication in 10 ml of distilled water. This dispersed NPs solution was mixed with magnetically stirred hot EG dissolved $La(NO_3)_3{\times}6\,H_2O$ (0.500 g) solution. After thirty minutes, an equal molar aqueous solution of NH_4F was introduced into the foregoing mixed system under magnetic stirring at 80 °C. Afterward, this suspension was refluxed at 80 °C for 3 h, until the complete precipitation occurred. The white precipitates were centrifuged and washed many times with ethanol and distilled water to remove excess unreacted reactants. The core/shell NPs were collected after centrifugation and were then dried at ambient temperature for further characterization.

2.4. Preparation of $LaF_3:Nd^{3+}@LaF_3@SiO_2$ NPs

The $LaF_3:Nd^{3+}@LaF_3@SiO_2$ core/shell NPs were prepared through a versatile Stober method as follows [9,21,23]. The synthesized $LaF_3:Nd^{3+}@LaF_3$ NPs

(50 mg) were well dispersed in a mixed solution of deionized water (50 ml), ethanol (70 ml) and concentrated aqueous ammonia (1.0 ml) in a three-neck round-bottom flask. Afterward, 1.0 ml of TEOS was added dropwise in 2 min, and the reaction was allowed to proceed for 6–7 h under continuous mechanical stirring. After stirring at room temperature, the silica-coated $LaF_3:Nd^{3+}@LaF_3$ core/shell NPs were separated by centrifugation, washed several times with ethanol and dried at room temperature for further analysis.

2.5. Characterization

Powder X-ray diffraction (XRD) analysis was performed at room temperature with the use of Rigaku X-ray diffractometer equipped with a Ni filter using Cu K_α (λ = 1.54056 Å) radiations. The morphologies of the samples were inspected using the field-emission transmission electron microscope (FE-TEM) equipped with an EDX (FETEM, JEM-2100F, JEOL, Japan) operating at an accelerating voltage of 200 kV. FTIR spectra were recorded with the Perkin-Elmer 580B IR spectrometer using KBr pellet technique in the range 4000–400 cm^{-1}. The UV-Vis absorption spectra were measured by Cary 80 spectrophotometer in the range of 190–600 nm. The photoluminescence spectra were recorded with Horiba Synapse 1024×256 pixels, where size of the pixel: 26 microns, detection range: 300 (efficiency 30%) to 1000 nm (efficiency 35%). In all the measurements, a slit width of 100 microns as employed, ensuring a spectral resolution better than 1 cm^{-1}.

III. Results and discussion

X-ray diffraction analysis was performed to examine the phase purity, crystal structure and crystalline size of the as-prepared products. All four samples exhibit all reflection planes of pure crystalline hexagonal phase LaF_3 (space group: *P3cl* (165)) as it can be seen from Fig. 1, which are consistent with the ICDD No. 32-0483 and other literature data [24–26]. No second phase corresponding to an impurity was detected in the XRD patterns revealing that Nd^{3+} has been effectively doped into the host lattice of hexagonal LaF_3 NPs. As shown in Fig. 1a, all reflection peaks are broad, revealing the nanocrystalline nature of the sample. However, the diffraction peak intensities have gradually increased with decreasing bandwidth after substantial growth of crystalline LaF_3 and an amorphous silica layer. This could be attributed to the systematic increase in the grain size of the nanomaterials after each surface modification. Furthermore, this finding is also indicating the successful surface coating around the core-NPs. Moreover, the characteristic peak of silica was not detected after one surface coating process, which may be due to thinner thickness and amorphous nature of the grafted silica layer. The average grain sizes of core, core/shell

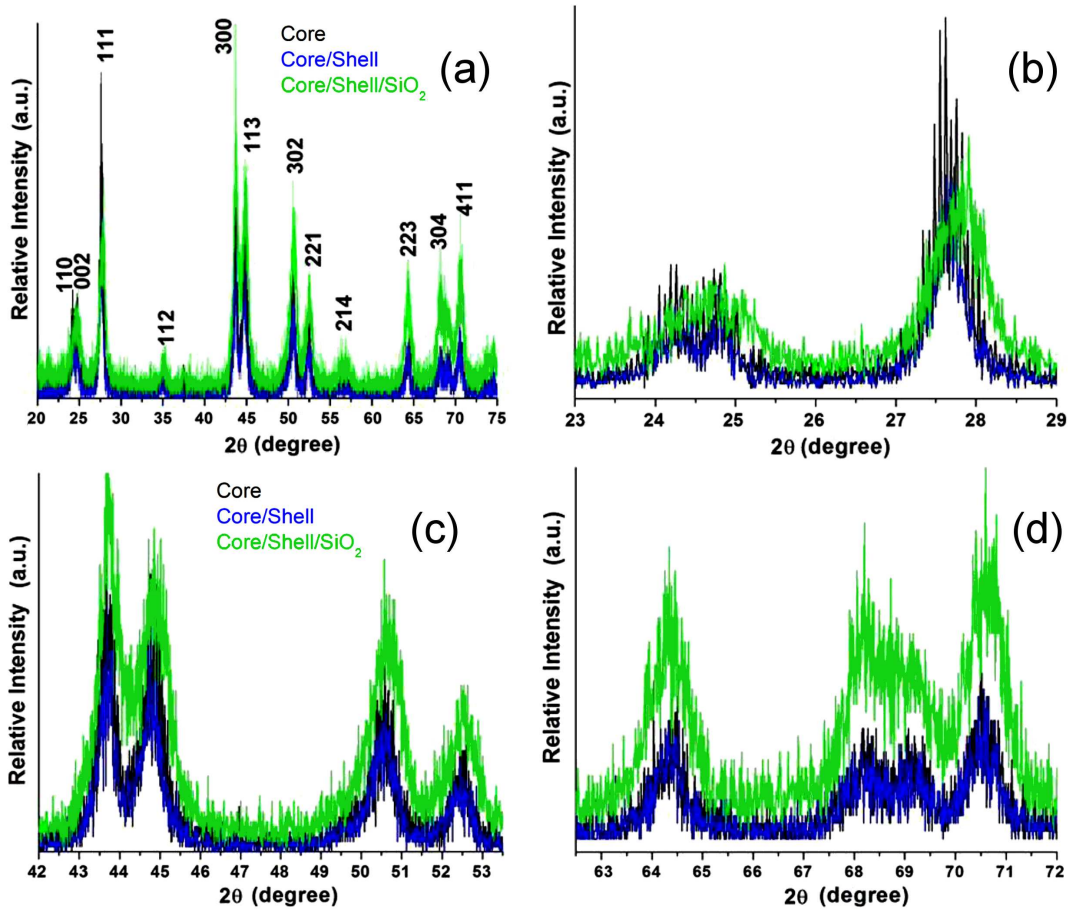

Figure 1. X-ray diffraction patterns of core, core/shell and core/shell/SiO_2 nanoparticles (a) - selected 2θ regions (b,c,d)

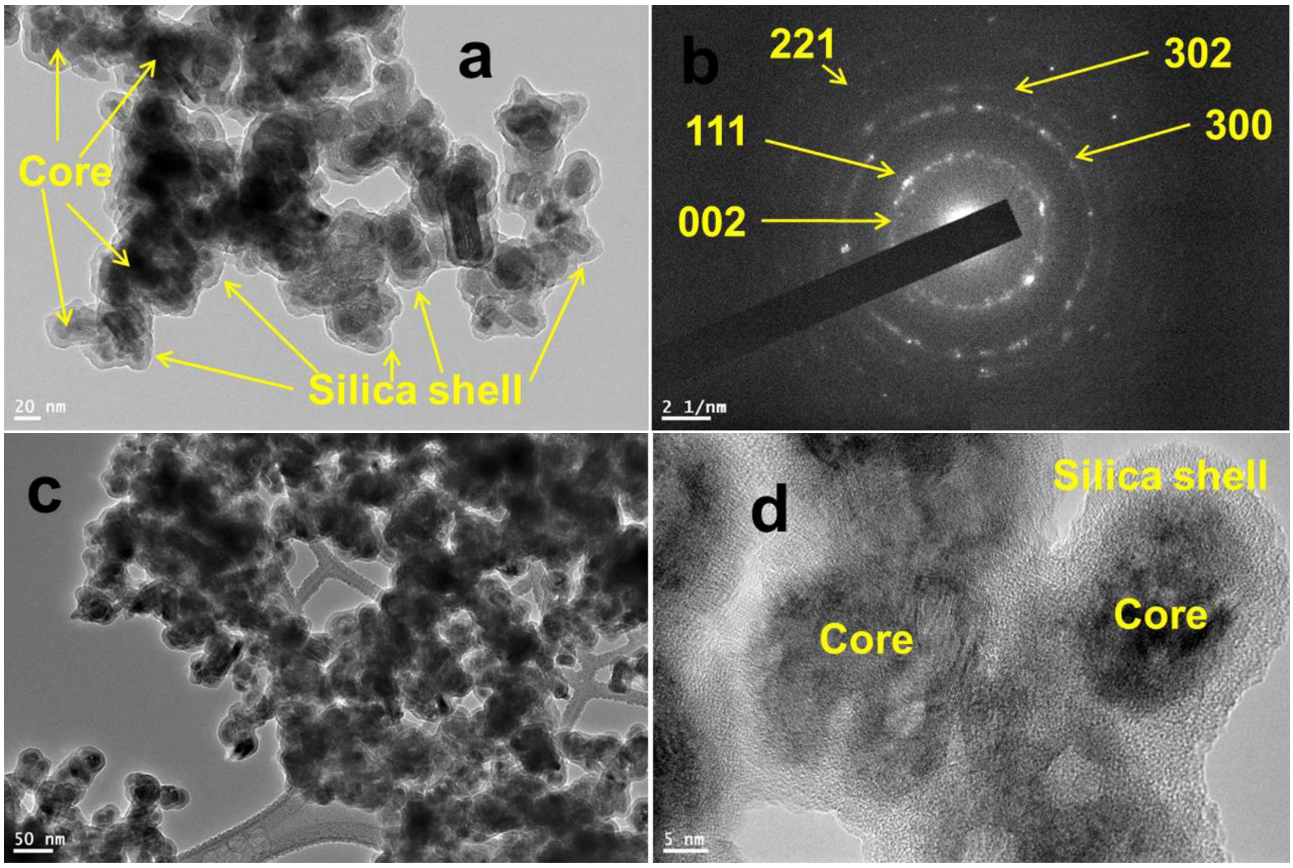

Figure 2. TEM images (a,c,d) and SAED pattern (b) of core/shell/SiO_2 nanoparticles

and core/shell/SiO_2 NPs calculated from the most strong XRD peaks at 111, 300 and 113 using the Scherrer formula are 10, 20 and 25 nm, respectively. The epitaxial growth of the crystalline LaF_3 and amorphous silica layers are the main reason for the increase in the crystal size and improvement in crystallinity as observed from sharp diffraction peaks (Fig. 1).

Transmission electron microscopy (TEM) images provide further evidence for the silica surface modification of the core/shell-NPs. As shown in Fig. 2, the size of each non-modified nanoparticle is in the range 10–20 nm whereas the sizes of the silica modified core/shell/SiO_2 NPs, which are observed as agglomerated NPs, can even go up to 20–30 nm. The aggregation is mainly attributed to the property of surface covered amorphous silica; in which surface silanol (Si–OH) groups enhance hydrogen bonding as well as Van der-Waal forces in aqueous solvents and these bonding along with large specific surface area of the silica modified core/shell/SiO_2 NPs increase aggregation in aqueous solvents. Furthermore, as the NPs are prepared in an aqueous environment at room temperature, their surface may be covered by a large number of hydroxyl groups either chemically bonded or physically adsorbed to the surface. In that case, water molecules may be adsorbed onto the NPs as a ligand coordinating with lanthanide ions. This was confirmed by the FTIR spectra as shown in Fig. 5. These hydroxyl groups and H_2O render the NPs water-soluble. It can be clearly seen from Figs. 2a and 2c that the smooth and uniform amorphous silica shell was successfully grafted over the irregularly shaped core/shell NPs. No evidence of non-silica coated core-NPs or pure silica core-nanospheres is observed in the TEM micrograph. The silica surface coating can be clearly distinguished by colour, where the luminescent core is dark black and silica is in light gray colour with a smooth surface (Fig. 2d). As seen in Fig. 2a, the luminescent core-NPs display mean diameter about 15 nm while the thickness of the silica shell is found to be about 8 nm yielding an overall diameter of around 27 nm for the coated particles. Figures 2a and 2c show the size of the core/shell/SiO_2 NPs and their monodispersity. The selected area electron diffraction (SAED) patterns of the core/shell/SiO_2 also confirm that luminescent core structures are crystalline and SiO_2 shell structures are non-crystalline (Fig. 2b). A high-resolution TEM image of the core/shell/SiO_2 NPs reveals their crystalline nature (Fig. 2a), and the SAED pattern (Fig. 2b) of the corresponding sample confirms that these luminescent core-NPs are in hexagonal structure with poly-crystallinity. The SAED pattern (Fig. 2b) shows the polycrystalline diffraction rings corresponding to the specific (002), (111), (300), (302) and (221) planes of the hexagonal LaF_3 lattice (ICDD No. 32-0483) [24–26] and therefore indicates that the obtained NPs are all highly crystalline and maintain the same hexagonal crystal structure during the synthesis process and are in good agreement with the observed X-ray

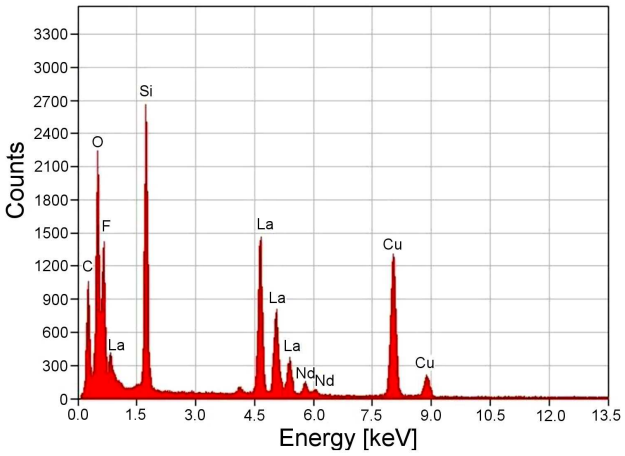

Figure 3. EDX spectrum of core/shell/SiO_2 NPs

diffraction results. EDX analysis was also performed to examine the surface silica coating on the core NPs (Fig. 3). The EDX analysis confirmed the presence of doped constituents such as La, F, O, Nd and Si in the host nanophosphor samples. These observations provide additional evidence for the formation of core/shell/SiO_2 nanostructure. The strong C and Cu signals observed in EDX were from carbon-coated copper TEM grid.

Figure 4 illustrates the thermogravimetric analysis of the as-prepared core, core/shell and core/shell/SiO_2 NPs from room temperature to 900 °C under nitrogen atmosphere. From the TGA curves of the core and core/shell NPs, approximately 6% and 3.5% weight loss was observed in first stage in the temperature range of 25–400 °C, which correspond to loss of organic moieties (EG) or dehydration of crystalline water molecules present on the surface of the core and core/shell NPs. After 400 °C, TGA curve exhibits a sluggish weight loss of up to 900 °C, which could be due to burn or elimination of surface-linked CO_2. Notably, TGA of the core/shell NPs exhibit high thermal stability with respect to the core NPs, indicating that the inert crystalline LaF_3 shell has been successfully grafted around the core NPs. However, the silica surface modified

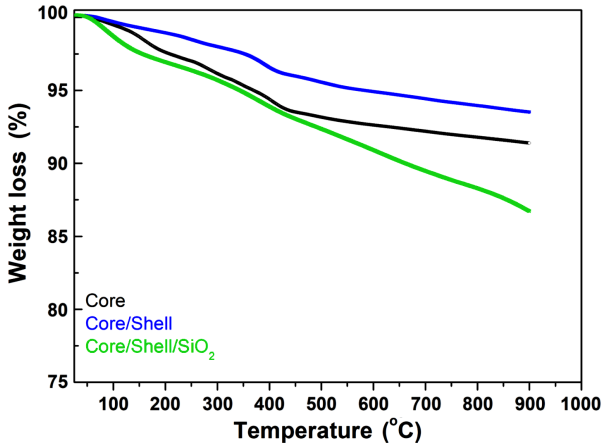

Figure 4. Thermal analysis of the core, core/shell and core/shell/SiO_2 nanoparticles

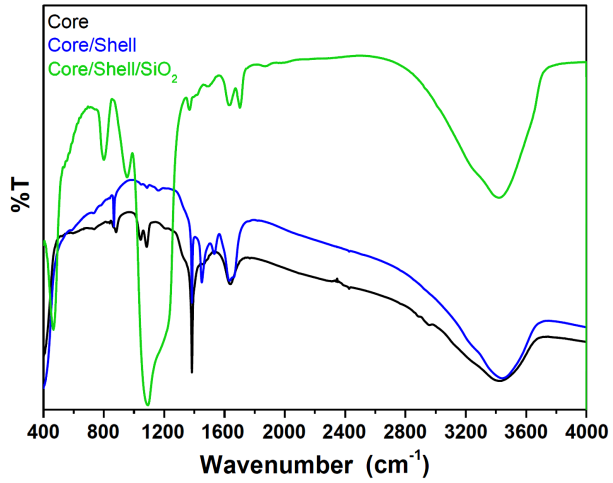

Figure 5. FTIR spectra of the core, core/shell and core/shell/SiO_2 nanoparticles

core/shell/SiO_2 NPs reveals two stages decomposition. First, weight loss took place in between 25–400 °C around 6% weight loss in the TGA curve, which was ascribed to the evaporation of water molecules on the surface of NPs. The second stage weight loss is associated with the combustion or burning of surface silica, transforming them into crystalline form or silicate.

FTIR spectroscopy was performed to verify the grafting of amorphous silica surface and attached surface functional groups as well as to analyse the hydrophobicity of the as-prepared samples. As shown in Fig. 5, FTIR spectra displayed main characteristic infrared absorption bands before and after shell formation around the core-NPs. The asymmetric, symmetric stretching, bending and wagging vibration modes of physically absorbed residual water bands appeared at around 3400, 1640 and 1430 $^{-1}$, respectively and were assigned to hydroxyl groups (O–H) [21,23]. A strong doublet infrared absorption band at around 1080 $^{-1}$ and two weak intensity peaks at 798 and 463 $^{-1}$ corresponding to the stretching and bending vibration modes of surface modified amorphous silica (Si–O, Si–O–Si, and Si–OH groups) were also observed [27]. These observations suggest that the amorphous silica has been successfully grafted around the core/shell NPs as verified by the TEM and EDX.

Optical properties, solubility, and colloidal stability characters of the as-prepared samples were probed by UV-Vis spectroscopy. Fig. 6 illustrates the absorption spectra of core, core/shell and core/shell/shell NPs in distilled water over the range of 200–600 nm. As seen in Fig. 6, a significant enhancement and redshift in absorption edge was observed due to optically active silica that has been grafted to the surface of core/shell NPs. We observed a similar trend in the absorption spectra measured in absolute ethanol. It was also confirmed by FTIR spectroscopy that the surface of prepared samples is covered by a large number of hydroxyl groups which render them aqueous-soluble. These surface hydroxyl groups play an important role for functionalization and

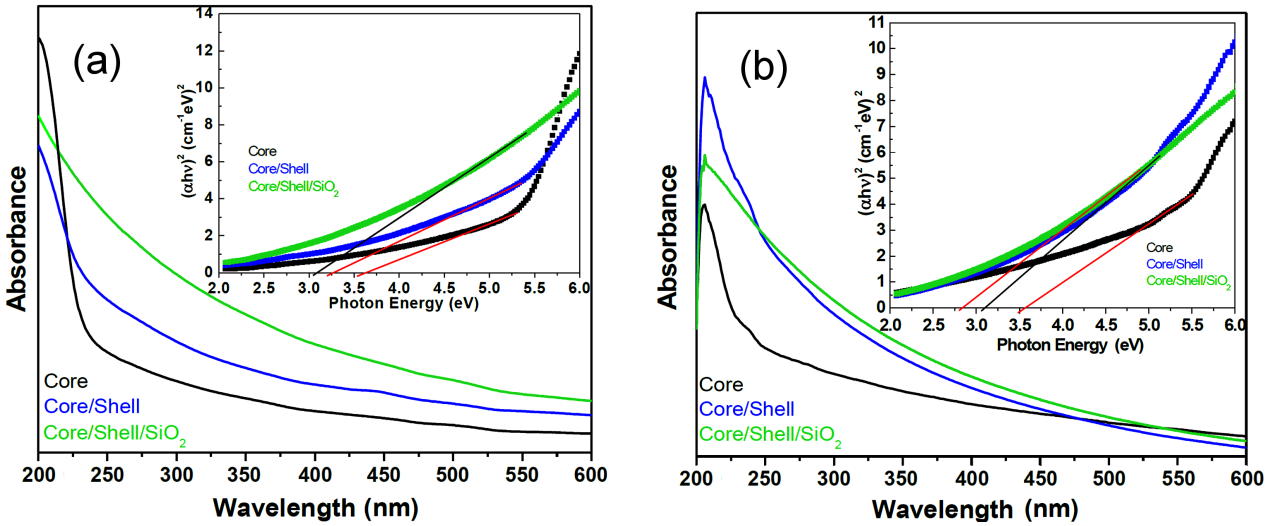

Figure 6. UV-Vis absorption spectra of the core, core/shell and core/shell/SiO_2 nanoparticles suspended in: a) de-ionized water and b) absolute ethanol (inset shows the plot of $(\alpha h\nu)^2$ vs. photon energy ($h\nu$))

their further use in biological systems that demand biocompatibility and non-toxicity. Furthermore, we analysed optical absorption spectra to examine the band gap energy of the as-synthesized nanophosphors and, thus, to reveal the correlation between band gap energy and the crystalline size of the nanoproducts. The band gap energy was determined from the sharply increasing absorption region according to Tauc and Menth law [28]. The inset of Fig. 6 shows the $(\alpha h\nu)^2$ versus the photon energy ($h\nu$) plots, where experimentally calculated band gap energy for the core, core/shell and core/shell/SiO_2 NPs are 3.62, 3.25 and 3.07 eV in H_2O and 3.55, 3.08 and 2.83 eV in absolute ethanol, respectively. It is observed that band gap energy has gradually decreased after surface grafting of core NPs indicating that surface coating brought an increase in the grain size of the nanophosphors. This result was also supported by the XRD, TEM, TGA and FTIR observations.

Figure 7 displays the photoluminescence spectra of the Nd^{3+}-doped LaF_3 (core), core/shell and core/shell/SiO_2 NPs excited at 325-nm wavelength to confirm the Nd^{3+} ion doping into the LaF_3 crystal lattice at similar quantity and measurement conditions. Several well-resolved emission peaks were observed at 542, 592, 636, 672-686, 722-753, 760-775 and 785-800 nm corresponding to the transitions from ($^2K_{15/2}$, $^2G_{9/2}$, $^2D_{3/2}$, $^2P_{3/2}$, $^4G_{11/2}$, $^2D_{1/2}$, $^2D_{5/2}$), ($^2K_{13/2}$, $^4G_{7/2}$, $^4G_{9/2}$), ($^2G_{7/2}$, $^4G_{5/2}$), ($^4F_{9/2}$), ($^4F_{7/2}$, $^4S_{3/2}$), ($^2H_{9/2}$, $^4F_{5/2}$) and ($^4F_{3/2}$) to the ground state $^4I_{9/2}$ of Nd^{3+}, respectively [2,7,10,13,14,16]. The obtained peaks were assigned to the energy levels of Nd^{3+} [2,7,10,13,14]. The shapes and peak positions of all emission transitions are similar in the core/shell and core/shell/SiO_2 NPs, which could be due to the similarity of crystal structures of the as-prepared nanomaterials, which were not altered after surface growth of crystalline passive LaF_3 and silica layers. In all the samples, the emission transition ($^4G_{5/2}$, $^2G_{7/2}$) located at 635 is the most intense which is due to its hypersensitive character [2,10,29]. This behaviour is in sharp contrast with other typically weak and consistently unvaried normal $4f$–$4f$ transitions. The highest peak belongs to the highest energetic one and intensities of other lines are smaller and gradually shifting to longer wavelengths. Three other emission transitions $^4F_{3/2}\rightarrow{}^4I_{9/2}$ (900 nm), $^4F_{3/2}\rightarrow{}^4I_{11/2}$ (1045–1080 nm) and $^4F_{3/2}\rightarrow{}^4I_{13/2}$ (1300–1450 nm) were not able to be recorded due to the limited spectral range of the spectrofluorometer. As seen in Fig. 7, the emission transitions bandwidth are much broader in the core/shell/SiO_2 NPs than their respective core and core/shell NPs. In the case of core/shell/SiO_2 NPs, a high intensity and broader band is observed between 400–500 nm range, which could be caused by silica emission (Fig. 7).

When the LaF_3:Nd NPs were coated with LaF_3 shell, the emission intensity is remarkably increased. The significant increase in the luminescence of NPs can be attributed to the beneficial influences of the LaF_3 shells. Additionally, it verifies the passivation role of the LaF_3 inert-shell, which protects the Nd^{3+} ions in the luminescent cores from non-radiative transitions caused by surface defects [19,20,30]. However, the emission intensity has greatly changed after the growth of an amorphous silica layer. The remarkable quenching in the emission spectrum can be attributed to the successful modification by the silica surface. The amorphous silica layer has a large number of silane (Si–OH) functional groups surrounding the core/shell NPs, which scatters the incident and emission light and thus suppress the emission intensity [28–30]. Furthermore, this high phonon energy species (Si–OH) and/or large amount surface density defects act as radiation traps which enhance the non-radiative transition rate causing the reduction of emission intensity. Moreover, it is particularly relevant to point out that lanthanide ion-doped NPs may also exhibit surface lanthanide species. This would then cause

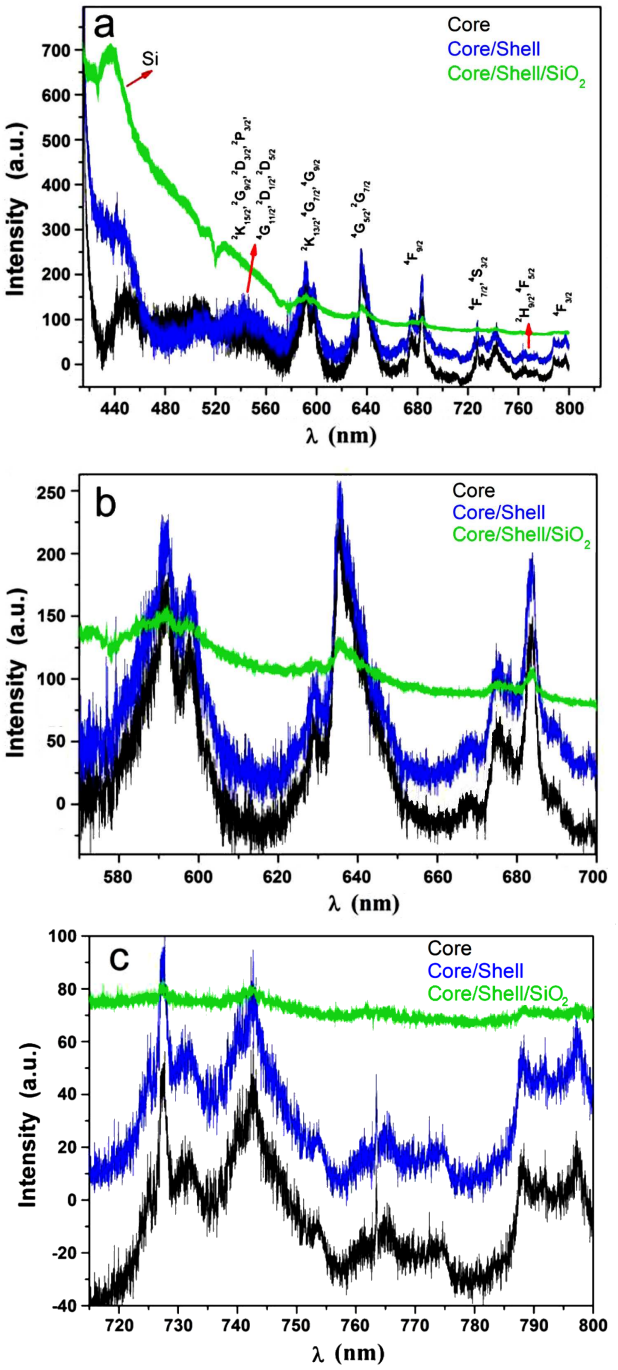

Figure 7. Photoluminescence spectra of the core, core/shell and core/shell/SiO_2 nanoparticles

the inter-ionic spacing to be small and hence quench emission transitions. Lastly, aqueous solubility and colloidal stability of the as-prepared luminescent seed NPs are crucial for their application in luminescent biological tags, since the NPs will be exposed to several biological fluids.

IV. Conclusions

Highly dispersed and pure hexagonal phase of LaF_3:Nd (core) and core/shell NPs were prepared successfully using co-precipitation process and then coated with an amorphous silica layer to form core/shell/SiO_2 NPs. XRD and TEM images clearly revealed the nanocrystalline size with irregular spherical shaped NPs with an average crystallite size of 21 nm. TEM images showed that the amorphous silica layer has been effectively grafted around the core/shell NPs, which was confirmed by FTIR spectral study. The optical properties of the NPs were greatly affected by the silica layer encapsulation because of the influence of the surface reform. This is ascribed to the formation of a large number of silanol functional groups that enhance the non-radiative transition rates and suppress emission intensity. These surface silanol functional groups have assisted in improving their solubility and colloidal stability in aqueous solvents. The as-prepared core/shell/SiO_2 NPs have tremendous potential applications in biolabeling and photonics-based bio-devices.

References

1. G.Y. Chen, T.Y. Ohulchanskyy, S. Liu, W.C. Law, F. Wu, M.T. Swihart, H. Agren, P.N. Prasad, "Core/shell $NaGdF_4:Nd^{3+}/NaGdF_4$ nanocrystals with efficient near-infrared to near-infrared downconversion photoluminescence for bioimaging applications", *ACS Nano*, **6** (2012) 2969–2977.
2. X.W. Zhang, Z. Zhao, X. Zhang, D.B. Cordes, B. Weeks, B.S. Qiu, K. Madanan, D. Sardar, J. Chaudhuri, "Magnetic and optical properties of $NaGdF_4:Nd^{3+}$, Yb^{3+}, Tm^{3+} nanocrystals with upconversion/downconversion luminescence from visible to the near-infrared second window", *Nano Res.*, **8** (2015) 636–648.
3. D.Q. Chen, L. Liu, P. Huang, M.Y. Ding, J.S. Zhong, Z.G. Ji, "Nd^{3+}-sensitized Ho^{3+} single-band red upconversion luminescence in core shell nanoarchitecture", *J. Phys. Chem. Lett.*, **6** (2015) 2833–2840.
4. X.M. Li, R. Wang, F. Zhang, L. Zhou, D.K. Shen, C. Yao, D.Y. Zhao, "Nd^{3+} sensitized up/down converting dual-mode nanomaterials for efficient in-vitro and in-vivo bioimaging excited at 800 nm", *Sci. Rep.*, **3** (2013) 3536.
5. J.J. Zhou, N. Shirahata, H.T. Sun, B. Ghosh, M. Ogawara, Y. Teng, S.F. Zhou, R.G.S. Chu, M.R. Fujii, J.R. Qiu, "Efficient dual-modal NIR-to-NIR emission of rare earth ions co-doped nanocrystals for biological fluorescence imaging", *J. Phys. Chem. Lett.*, **4** (2013) 402–408.
6. U. Rocha, C. Jacinto, W.F. Silva, I. Guedes, A. Benayas, L.M. Maestro, M.A. Elias, E. Bovero, F.C.J.M. van Veggel, J.A.G. Sole, D. Jaque, "Subtissue thermal sensing based on neodymium-doped LaF_3 nanoparticles", *ACS Nano*, **7** (2013) 1188–1199.
7. X.F. Yu, L.D. Chen, M. Li, M.Y. Xie, L. Zhou, Y. Li, Q.Q. Wang, "Highly efficient fluorescence of NdF_3/SiO_2 core/shell nanoparticles and the applications for in vivo NIR detection", *Adv. Mater.*, **20** (2008) 4118–4123.
8. U. Rocha, K.U. Kumar, C. Jacinto, I. Villa, F. Sanz-Rodriguez, M.D.I. de la Cruz, A. Juarranz, E. Carrasco, F.C.J.M. van Veggel, E. Bovero, J.G. Sole, D. Jaque, "Neodymium-doped LaF_3 nanoparticles for fluorescence bioimaging in the second biological window", *Small*, **10** (2014) 1141–1154.
9. S. Sivakumar, P.R. Diamente, F.C. van Veggel, "Silica-coated Ln^{3+}-doped LaF_3 nanoparticles as robust down-

and upconverting biolabels", *Chem. Eur. J.*, **12** (2006) 5878–5884.
10. M. Li, Z.H. Hao, X.N. Peng, J.B. Li, X.F. Yu, Q.Q. Wang, "Controllable energy transfer in fluorescence upconversion of NdF_3 and $NaNdF_4$ nanocrystals", *Optics Express*, **18** (2010) 3364–3369.
11. A.A. Ansari, N. Singh, A.F. Khan, S.P. Singh, K. Iftikhar, "Solvent effect on optical properties of hydrated lanthanide tris-acetylacetone", *J. Luminescence*, **127** (2007) 446–452.
12. A.A. Ansari, M. Irfanullah, K. Iftikhar, "Optical absorption and NMR spectroscopic studies on paramagnetic neodymium(III) complexes with beta-diketone and heterocyclic amines - The environment effect on 4f-4f hypersensitive transitions", *Spectrochim. Acta Part A - Mol. Biomol. Spectroscopy*, **67** (2007) 1178–1188.
13. M. Guzik, E. Tomaszewicz, Y. Guyot, J. Legendziewicz, G. Boulon, "Structural and spectroscopic characterizations of two promising Nd-doped monoclinic or tetragonal laser tungstates", *J. Mater. Chem.*, **22** (2012) 14896–14906.
14. E. Steveler, H. Rinnert, M. Vergnat, "Direct and indirect excitation of Nd^{3+} ions sensitized by Si nanocrystals embedded in a SiO_2 thin film", *J. Appl. Phys.*, **110** (2011) 113518.
15. X.X. Cui, J.B. She, C. Gao, K. Cui, C.Q. Hou, W. Wei, B. Peng, "Luminescent properties of Nd^{3+}-doped LaF_3 core/shell nanoparticles with enhanced near infrared (NIR) emission", *Chem. Phys. Lett.*, **494** (2010) 60–63.
16. M.Y. Xie, L. Yu, H. He, X.F. Yu, "Synthesis of highly fluorescent LaF_3:Ln^{3+}/LaF_3 core/shell nanocrystals by a surfactant-free aqueous solution route", *J. Solid State Chem.*, **182** (2009) 597–601.
17. G.A. Kumar, C.W. Chen, J. Ballato, R.E. Riman, "Optical characterization of infrared emitting rare-earth-doped fluoride nanocrystals and their transparent nanocomposites", *Chem. Mater.*, **19** (2007) 1523–1528.
18. L. Gui, X.X. Cui, W. Wei, B. Peng, D.Y. Fan, "Effects of different ligands on luminescence properties of LaF_3:Nd nanoparticles", *J. Rare Earths*, **31** (2013) 645–649.
19. A. Kar, A. Patra, "Impacts of core-shell structures on properties of lanthanide-based nanocrystals: crystal phase, lattice strain, downconversion, upconversion and energy transfer", *Nanoscale*, **4** (2012) 3608–3619.
20. A.K. Parchur, A.I. Prasad, A.A. Ansari, S.B. Rai, R.S. Ningthoujam, "Luminescence properties of Tb^{3+}-doped $CaMoO_4$ nanoparticles: annealing effect, polar medium dispersible, polymer film and core-shell formation", *Dalton Trans.*, **41** (2012) 11032–11045.
21. A.A. Ansari, S.P. Singh, N. Singh, B.D. Malhotra, "Synthesis of optically active silica-coated NdF_3 core-shell nanoparticles", *Spectrochim. Acta Part A - Mol. Biomol. Spectroscopy*, **86** (2012) 432–436.
22. X. Tang, E. Kroger, A. Nielsen, C. Strelow, A. Mews, T. Kipp, "Ultrathin and highly passivating silica shells for luminescent and water-soluble CdSe/CdS nanorods", *Langmuir*, **33** (2017) 5253–5260.
23. A.A. Ansari, M. Alam, J.P. Labis, S.A. Alrokayan, G. Shafi, T.N. Hasan, N.A. Syed, A.A. Alshatwi, "Luminescent mesoporous $LaVO_4$:Eu^{3+} core-shell nanoparticles: synthesis, characterization, biocompatibility and their cytotoxicity", *J. Mater. Chem.*, **21** (2011) 19310–19316.
24. F. Wang, Y. Zhang, X.P. Fan, M.Q. Wang, "One-pot synthesis of chitosan/LaF_3:Eu^{3+} nanocrystals for bioapplications", *Nanotechnol.*, **17** (2006) 1527–1532.
25. R. Mangaiyarkarasi, S. Chinnathambi, P. Aruna, S. Ganesan, "Synthesis of 5-fluorouracil conjugated LaF_3:Tb^{3+}/PEG-COOH nanoparticles and its studies on the interaction with bovine serum albumin: spectroscopic approach", *J. Nanoparticle Res.*, **17** (2015) 136.
26. F. Wang, Y. Zhang, X.P. Fan, M.Q. Wang, "Facile synthesis of water-soluble LaF_3:Ln^{3+} nanocrystals", *J. Mater. Chem.*, **16** (2006) 1031–1034.
27. A.A. Ansari, T.N. Hasan, N.A. Syed, J.P. Labis, A.K. Parchur, G. Shafi, A.A. Alshatwi, "In-vitro cytotoxicity, geno-toxicity, and bio-imaging evaluation of one-pot synthesized luminescent functionalized mesoporous SiO_2@$Eu(OH)_3$ core-shell microspheres", *Nanomed. Nanotechnol.*, **9** (2013) 1328–1335.
28. J. Tauc, A. Menth, "States in the gap", *J. Non-Cryst. Solids*, **8** (1972) 569–585.
29. A.A. Ansari, R. Ilmi, K. Iftikhar, "Hypersensitivity in the 4f-4f absorption spectra of tris (acetylacetonato) neodymium(III) complexes with imidazole and pyrazole in non-aqueous solutions. Effect of environment on hypersensitive transitions", *J. Luminescence*, **132** (2012) 51–60.
30. F. Vetrone, R. Naccache, V. Mahalingam, C.G. Morgan, J.A. Capobianco, "The active-core/active-shell approach: A strategy to enhance the upconversion luminescence in lanthanide-doped nanoparticles", *Adv. Funct. Mater.*, **19** (2009) 2924–2929.